Varying Magnet Type and Stack Length in a Surface PM Soft Magnetic Composite Machine

Yik Ling Lim, Wen L. Soong, Nesimi Ertugrul and Gabriel Haines

***Abstract* – This paper examines the effect of varying the magnet type and stack length of a surface PM machine using soft magnetic composite pole-pieces. Firstly, the finite-element modelling and testing of a 9 slot, 8 pole, 400 W machine with a bonded rare-earth magnet ring is described. Secondly, the use of alternative magnet types and the effect of stack length changes on the machine loss and material cost are investigated using a combination of analytical and finite-element results.**

***Index Terms* -- Brushless permanent magnet machines, finite-element analysis, permanent magnets, soft magnetic composites.**

I. INTRODUCTION

THREE types of brushless electrical machines (induction, reluctance, and permanent magnet (PM)) offer reliable performance in industrial applications. Although brushless PM machines can achieve high efficiency and high power density, they also cost more due to high magnet costs.

In brushless PM machines, the construction cost of the stator may be reduced by using soft magnetic composite (SMC) material. This is essentially iron powder particles coated with an electrically insulated layer that are moulded under high pressure in a die.

Only two-dimensional (2D) electromagnetic geometries can be achieved with conventional silicon-iron laminations. The isotropic nature of SMC however offers possibilities for 3D design solutions. Stator pole pieces made of SMC can be produced in a single step, unlike laminations, which require stamping and assembly. Thus SMC can have advantages such as better performance, reduced size and weight, fewer parts and lower cost [1-2].

A substantial component of the cost of brushless PM machines can be the PM material cost. Rare-earth PM materials have been commonly used due to their large energy product, allowing them to provide higher power density. However, the use of rare-earth PMs has become an issue because of substantial price fluctuations in recent years [3]. Recently, alternatives to using rare-earth PMs have been explored [4].

Ferrite PMs are abundant, available at low cost, and have negligible eddy current losses in low-frequency applications which makes them an attractive alternative to rare-earth magnets [5]. However, they have a much lower energy product (BH_{max}) than rare-earth magnets, which presents performance restrictions.

The main aim of this paper is to investigate different magnet options in an existing SMC based brushless PM machine with a target aim to lower both the production cost and magnet material cost.

Barcaro et al. [6] have studied the influence of magnet volume on motor performance in a PM-assisted synchronous reluctance machine. In this paper however, we deal with an existing surface PM machine with a fixed stator.

Another aim of the present paper is to investigate the effect of varying the machine stack length on performance, as the stack length determines the amount of material used in the manufacture of the machine and hence the machine cost.

Barcaro et al. [7] studied the effect of replacing surface PM machines using rare-earth PMs with interior PM machines using ferrite PMs. An increase in the stack length and an almost doubling of the PM volume was required, but the cost of the ferrite machine was still much lower than that of the rare-earth machine. Zarko et al. [8] have analysed the effect of varying stack length in devising a general approach to the optimized design of interior PM motors. However, the machine used in this paper is a surface PM machine.

Three different magnet and design types are considered in this paper: a bonded rare-earth neodymium-iron-boron (NdFeB) magnet ring, a sintered NdFeB magnet and a ferrite magnet. During the utilisation of these three magnet design options, the primary aim is to maintain the same machine performance (in terms of torque and speed) and to determine their limitations. In addition, the secondary aim is to reduce rotor losses.

Sintered rare-earth magnets are commonly used in many surface PM machine applications to obtain high torque density. However, sintered rare-earth magnets with concentrated stator windings can produce large eddy-current losses in the magnets. Segmenting the sintered magnets, or using bonded magnets, can decrease such losses. In addition, bonded ring magnets involve a simple rotor construction, since the individual magnet segments do not need to be assembled. Moreover, they have higher resistivity and their dimensional tolerances can be very small, but they have lower remanent flux density than sintered magnets. Therefore, this paper will investigate the three magnet options mentioned above to determine the best option for trading off machine cost against performance.

In this paper, section 2 describes the design information for the baseline SMC machine, and the finite-element (FE) modelling and experimental verification of the baseline machine with a bonded magnet rotor. In section 3, the effects of remanent magnet flux density and stack length on the machine loss versus load characteristics are analysed. Section 4 describes the FE modelling of the machine with the three rotor magnet options and compares the options. Finally, section 5 concludes the paper.

II. BASELINE MACHINE AND FINITE-ELEMENT MODELLING

A. Machine Configuration

The SMC machine investigated in this paper is an existing 400 W, 3,000 rpm, 8 pole, 9 slot surface PM machine utilising concentrated stator windings. Table I gives the key machine design information including the measured stator resistance.

The authors are with the School of Electrical and Electronic Engineering, The University of Adelaide, Australia (e-mail: yikling.lim@adelaide.edu.au).

TABLE I
KEY DESIGN DATA FOR BASELINE SMC MACHINE

Number of stator slots	9
Number of rotor poles	8
Stator core, SMC-Somaloy 550K - outer diameter - stack length	 90 mm 50 mm
Stator winding turns per phase	90 turns
Airgap length	1 mm
Packing factor	0.40
Rotor back-iron resistivity	2.22×10^{-7} Ωm
Stator phase resistance	0.275 ohms

The 3D advantage of the isotropic nature of SMC is utilized in the manufacture of the stator teeth. The body of the tooth of each pole is recessed so that the end-windings do not extend beyond the axial length of the stator back-iron. Thus the active stack length is equal to the physical stack length as shown in Fig. 1a.

Although 3D FE modelling of the machine would have led to more accurate analysis, 2D modelling was performed to reduce simulation time. The recessed pole pieces were approximated in a 2D model (see Fig. 1b) by reducing the width of each modelled tooth body by adding an air gap on either side to make the modelled magnetic tooth body area the same as that of the actual pole piece [2].

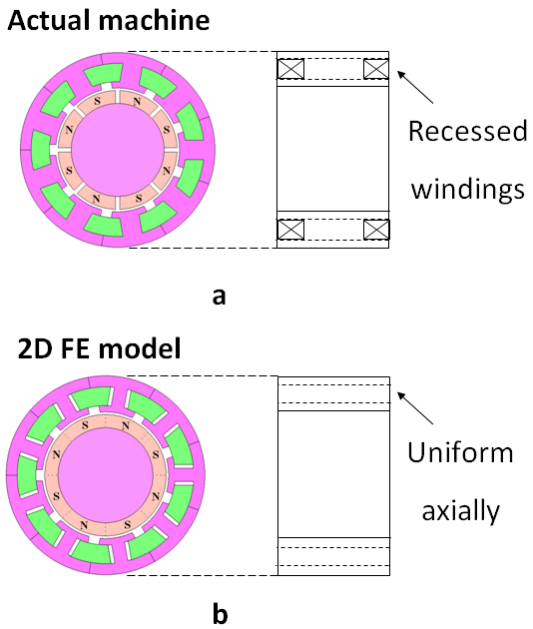

Fig. 1. (a) Actual machine with recessed windings (b) 2D FE model of machine with a narrower tooth body (air gap added) to account for the recessed 3D pole piece

B. *Rotor Options*

As this is an existing machine, the same stator is used throughout and thus the stator slot area remains constant. Therefore, only the rotor is modified to accommodate the different magnet materials. Table II summarises these rotor magnet options and their characteristic values, including estimated material cost. The magnet costs are relative to the cost of ferrite, which is set at 1 p.u.

The stator of a machine with a ferrite rotor magnet would have a lower airgap flux density and hence normally have a thinner tooth width (a 'copper' design) than that of a machine with an NdFeB rotor magnet (an 'iron' design). In this paper, we are restricted to existing SMC stator teeth mouldings. This study will involve the variation of stack length to compare the different rotor magnet options, although this would also require different moulds to be used.

The test machine uses the bonded NdFeB ring and all the different rotor magnet options are finite-element modelled and simulated.

TABLE II
COMPARISON OF PERMANENT MAGNET MATERIALS

	Ferrite	**Bonded NdFeB**	**Sintered NdFeB**
Remanent magnetic flux density (T)	0.47	0.71	1.4
Resistivity (Ωm)	2×10^{-4}	2×10^{-5}	1.5×10^{-6}
Density (g/cm^3)	4.9	6.0	7.4
Relative magnet cost, versus ferrite (p.u.)	1	5	10

C. *Finite-Element Modelling*

Two-dimensional finite-element modelling was used to analyse the characteristics of the SMC machine with a bonded NdFeB magnet ring rotor. This uses a ring magnet which has been selectively magnetised to have alternating north and south poles. The specifications follow those of Table I.

The model was simulated at a speed of 3000 rpm. The maximum induced phase voltage was found to be about 29 V rms, and the stator iron loss was approximately 33 W.

D. *Verification of Baseline Design*

A prototype SMC machine has been built with pressed SMC pole pieces. The rotor in the machine consists of an 8-pole bonded NdFeB magnet ring with a solid magnetic back-iron. The SMC machine was connected to a dc machine for driving and loading purposes.

The prototype machine was run at a range of speeds under open-circuit conditions. A back-emf constant of approximately line 0.147 V_{rms}/(rad/s) was obtained. At 3000 rpm, the induced line voltage was about 47 Vrms. This is comparable to that predicted by the FE modelling (about 50 Vrms). Fig. 2 shows the FE-predicted and experimental induced line back-emf waveforms.

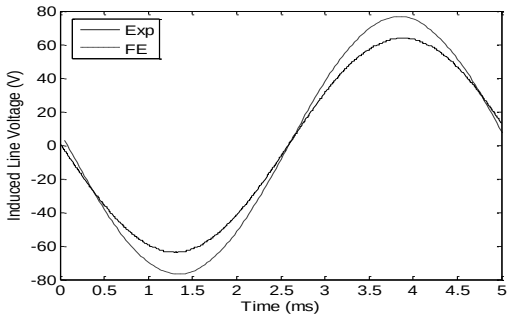

Fig. 2. Calculated and measured (experimental) induced line voltage at 3000 rpm.

The SMC machine was disconnected from the dc machine and the dc machine was spun alone to determine its no-load losses and back-emf constant. Next, the torque of the system with the SMC machine connected to the dc machine was found. The difference between the two tests gave the measured open-circuit loss for the SMC machine alone as shown in Fig. 3 along with the FE calculated stator and rotor iron loss. A difference of the order of a factor of two was observed. This is likely due to a combination of bearing/windage loss and errors in the iron loss model used.

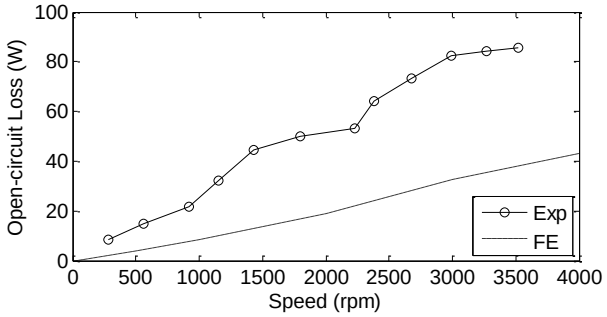

Fig. 3. Calculated iron loss and measured open-circuit loss of prototype SMC machine against speed

E. Performance Prediction

Having obtained the measured stator resistance, back-emf constant and open-circuit loss, it is possible to use these to predict the performance of the SMC machine. A calculated efficiency map for the SMC test machine is given in Fig. 4.

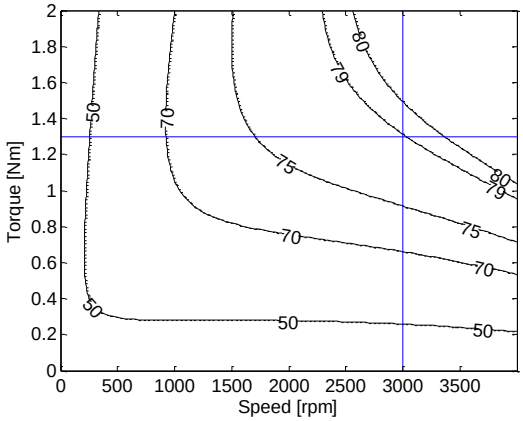

Fig. 4. Calculated efficiency map for the SMC machine, with the rated torque and speed shown

At the rated speed of 3000 rpm and rated torque of 1.3 Nm, the efficiency of the SMC test machine with the bonded NdFeB ring is about 79%.

III. Analytical Modelling of Effect of Varying Magnet Remanent Flux Density and Stack Length

An analytical modelling approach is used to analyse the effects of remanent magnetic flux density and stack length on the loss versus load characteristics of a surface PM machine at rated speed. For simplicity, it is assumed that the machine has equal iron and copper losses at rated speed and rated torque.

A. Varying Remanent Magnetic Flux Density

The iron loss is assumed to be only a function of speed and to be unaffected by the torque. For a surface PM machine the current is assumed to be proportional to torque and hence the copper loss is proportional to the square of the torque (or load).

Fig. 5 illustrates the breakdown of the machine loss into iron and copper losses as a function of load at rated speed. This shows a quadratic relationship between the copper loss and the load, with the vertical axis intercept equal to the iron loss.

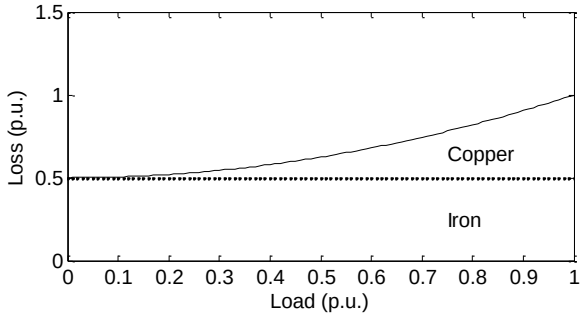

Fig. 5. Total loss (separated into iron and copper losses) versus load characteristic at rated speed expressed in p.u. relative to loss at full-load.

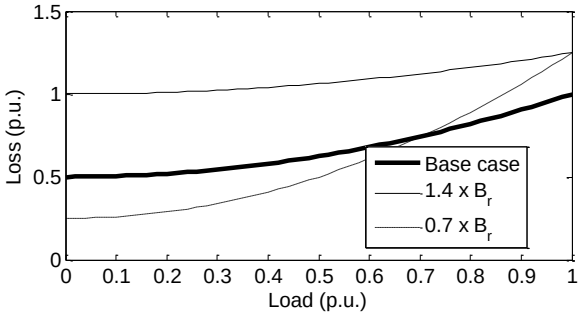

Fig. 6. Loss against load for three values of remanent magnetic flux density B_r

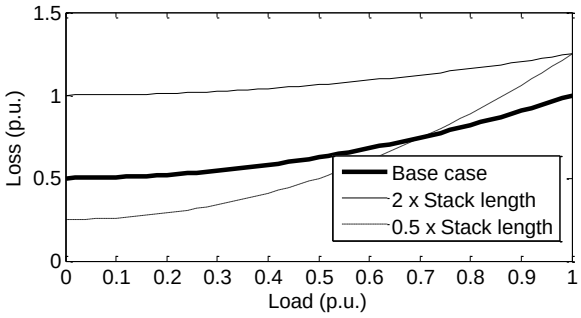

Fig. 7. Loss against load for three values of stack length

Note that the iron loss is made up of hysteresis loss and eddy current loss, both of which are proportional to B^2 and hence B_r^2 (to a first approximation). The iron loss is also proportional to the stack length L, so:

$$P_{Fe} \propto B_r^2 L \tag{1}$$

The induced voltage E is assumed to be proportional to the product of B_r and L. Assuming that E and the stator current I are in phase, the output power P is proportional to EI. The copper loss is proportional to I^2 and hence to $(P^2/E^2)L$. Since E^2 is proportional to $B_r^2L^2$, thus:

$$P_{Cu} \propto \frac{P^2}{B_r^2 L} \tag{2}$$

The output power of an electric machine is proportional to the product of the magnetic loading and the electric loading, or the product of the magnetic flux density and the current density. Since the stator dimensions of the reference machine are kept the same, if the rotor magnet material is changed from one with a higher B_r to one with a lower B_r, then the current and hence copper loss in the stator windings will need to increase to maintain the same torque.

Fig. 6 shows the losses for three different values of B_r': the base case (B_r' = B_r), B_r' = 1.4B_r and B_r' = 0.7B_r. Compared to the base case, the 0.7B_r machine has half the

no-load loss and lower loss for values of load below about 0.7 p.u, but the loss increases rapidly as load rises beyond this point.

Meanwhile, the $1.4B_r$ machine has twice the no-load loss than the base case, but the loss does not increase with load as quickly as that of the base case. Note that the effects of saturation have been neglected.

Thus lower B_r machines have lower losses at low load values, while higher B_r machines have lower loss at higher load values. Therefore, we expect that machines with ferrite rotors offer lower loss at low values of load than machines with rare earth magnet rotors.

B. Varying Stack Length

The effect of the end-winding copper loss and the 3D nature of the SMC teeth are ignored in this simplified analysis.

Varying the stack length of the machine has a significant impact on the losses suffered by the machine. Increasing the stack length will increase the iron losses proportionally. If the torque is maintained at the same level, the required electrical loading will decrease and hence the copper losses will be reduced. For example, a doubling of the stack length will result in a doubling of the iron losses and a halving of the current density. The copper losses will go down by a factor of 2 (a reduction by a factor of 4 due to the reduced current density multiplied by a factor of 2 due to the increased stack length).

Fig. 7 shows the relationship for several cases: a base case, a doubling of the stack length and a halving of the stack length. Comparing this with Fig. 6, note that halving the stack length has the same effect on the loss versus load curve as reducing the magnet remanent flux by 30%. Also doubling the stack length has the same effect as increasing the magnet flux by 40%. This is consistent with the results from (1) and (2).

Thus machines with shorter stack lengths give lower loss at low values of load while machines with longer stack lengths give lower loss at higher load values.

IV. Comparison of Rotor Magnet Options

The FE model results have been checked against the results of the experimental testing on the prototype baseline machine.

For the other two rotor magnet options, the same stator geometry and rotor outer diameter were used, while the rotor magnet remanent flux density was varied by varying the rotor magnet material and thickness. The effect of changing the machine stack length was also examined.

The bonded NdFeB ring and ferrite rotor magnets had a thickness of 6 mm, while the sintered NdFeB rotor magnet thickness was chosen to be half of this value (3 mm). For the sintered and ferrite magnets, a gap of 2 mm was assumed between magnets. Fig. 8 illustrates the rotors of the three machines.

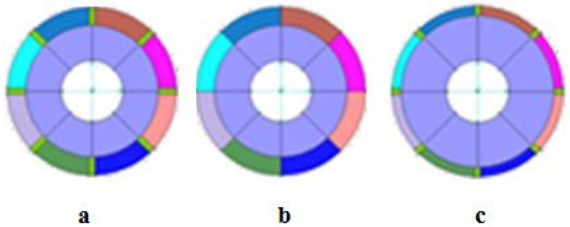

Fig. 8. FE models of (a) ferrite, (b) bonded NdFeB ring and (c) sintered NdFeB rotor

Fig. 9 and Fig. 10 show plots of induced voltage against remanent magnetic flux density and magnet cost for the three rotor magnet options. For a given magnet thickness the induced voltage is proportional to remanent flux density. The sintered NdFeB design uses thinner magnets and so has a lower ratio of induced voltage to remanent flux density. The ratio of the back-emf divided by the cost is lowest for ferrite.

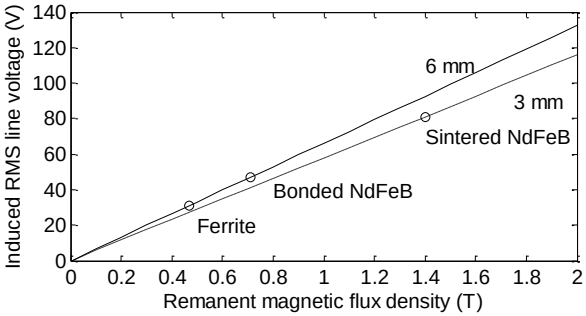

Fig. 9. Induced voltage (at 3000 rpm) against remanent magnetic flux density for the three rotor magnet options taking into the account the 6 mm and 3mm magnet thicknesses

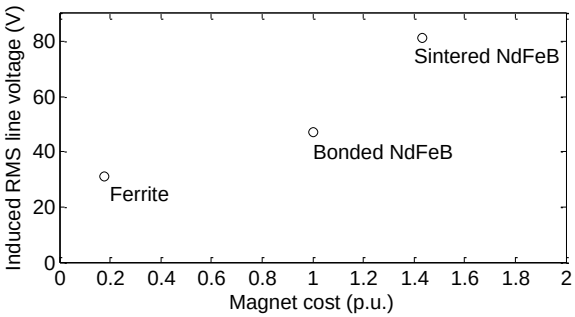

Fig. 10. Induced voltage against magnet cost for the three rotor magnet options, normalized to the bonded NdFeB magnet case

The iron, magnet and copper losses were calculated using FE modelling for the three options under no-load and full-load (400 W) conditions. The loss breakdowns are shown in Fig. 11.

From (1), the iron loss is ideally proportional to the square of the remanent flux density but interestingly the finite-element analysis results show closer to a linear relationship which may be associated with the SMC properties. This aspect needs further investigation.

Under no-load conditions, the magnet loss is due to magnet flux variations from the stator slot openings and is relatively small. It is most significant in the sintered design due to its low magnet resistivity. The magnet loss shows a small increase under full-load conditions due to the stator winding airgap flux density harmonics.

From (2), the copper losses are expected to be proportional to the square of the remanent flux density. The ferrite design shows the lowest calculated full-load losses at this value of output power.

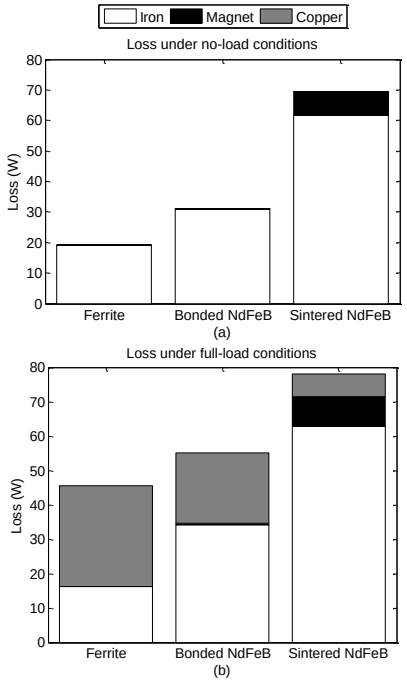

Fig. 11. Loss breakdowns under (a) no-load and (b) full-load conditions for the three rotor magnet options at 400 W and 3000 rpm

The iron, magnet and copper material weights and costs were calculated for the three rotor options and are shown in Fig. 12. The iron and copper costs are constant because it is assumed that the stack length is constant for the three options. The assumed costs ($/kg) relative to ferrite, are as follows: SMC 0.5 p.u., copper 1.1 p.u., and the magnet costs are given in Table II. As indicated in Fig. 12b, magnet costs make up the majority of the material costs when using rare-earth magnets. Relative to the baseline bonded machine, the sintered design is roughly twice the cost, while the ferrite machine is less than half the cost.

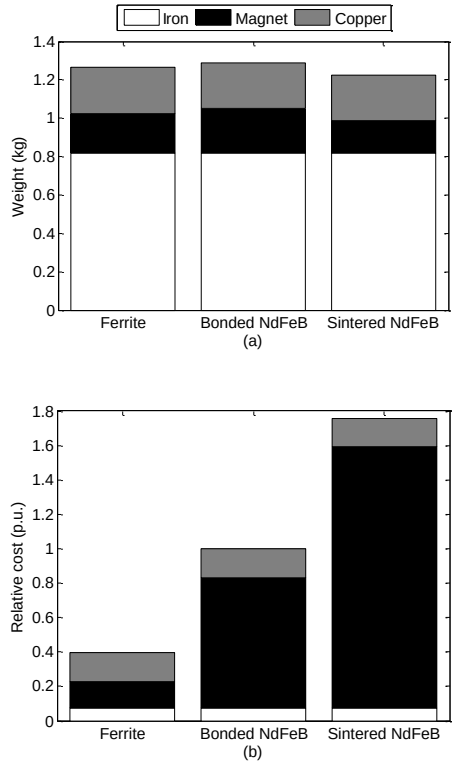

Fig. 12. Material breakdowns by (a) weight and (b) relative cost (normalized to the bonded NdFeB machine) for the three options

The total loss (iron, magnet and copper) can also be plotted against load, as shown in Fig 13. As expected from the earlier analytical modelling results, the lowest B_r material (ferrite) starts with the least loss but this increases the most rapidly with load, while the highest B_r material (sintered NdFeB) begins with the highest loss but this increases the most gradually with load. The load levels at which the designs have equal losses are about 450W for the ferrite and bonded designs and about 950 W for the bonded and sintered designs.

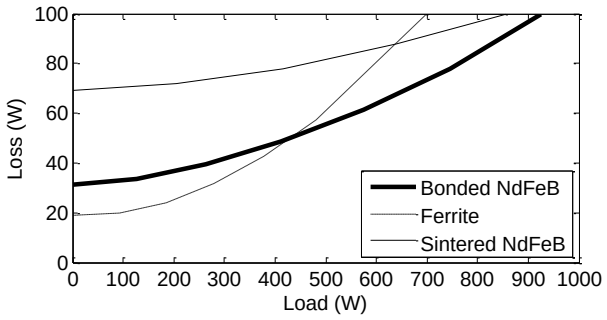

Fig. 13. Loss against load for the three rotor magnet options at 3000 rpm

For the bonded NdFeB base case, the stack length was varied to see how the loss against load curves vary with stack length as shown in Fig. 14. It was found that lower stack lengths resulted in lower loss at low values of load that increased more rapidly than the loss at higher stack lengths, which began at higher values of loss. This is a similar effect to varying the remanent magnetic flux density.

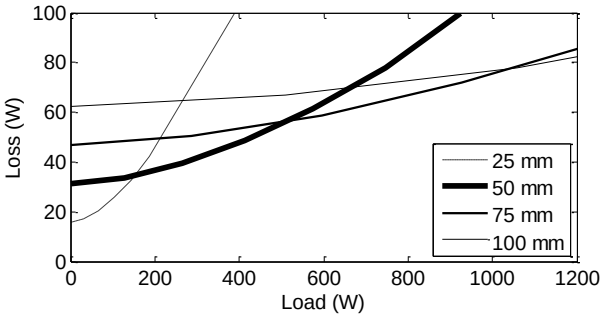

Fig. 14. Loss against load for the bonded NdFeB magnet option with a variety of stack lengths at rated speed.

A doubling of the stack length results in a doubling of the amount of iron, magnet and copper. The iron and magnet losses are doubled and also the back-emf, hence only half the current is required. Copper loss is proportional to I^2, so a halving of the current with a doubling of the amount of copper gives an overall halving of the copper loss. We see in Fig. 14 that doubling the stack length results in a higher initial loss due to the increased iron and magnet losses, but a more gradual rise in loss with load because of the decreased copper loss.

A plot of loss against stack length at full-load was obtained from analysis and broken down into iron, magnet and copper losses. The iron and magnet losses are assumed proportional to the stack length. As the load is assumed constant, the current and, as it turns out, also the copper loss are inversely proportional to the stack length, to a first approximation. Fig. 15 shows the breakdown of losses against stack length.

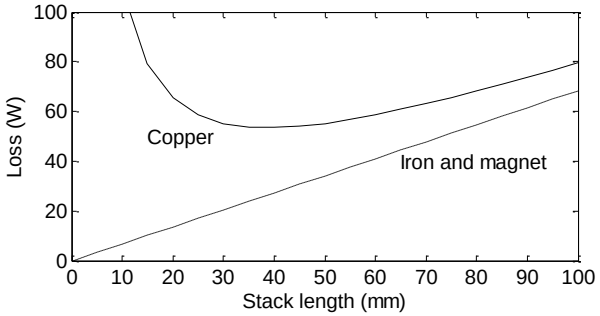

Fig. 15. Analytically calculated total loss against stack length showing the breakdown into copper, magnet and iron losses for the bonded NdFeB option

At low values of stack length, the copper loss dominates, while the iron and magnet losses increase linearly with stack length, as expected from the aforementioned relationships between the losses and the stack length. The minimum loss point corresponds to when the copper and iron losses are roughly equal.

It should be noted that the assumption of a linear variation of iron and magnet losses with stack length is simplistic. In practice, as the stack length is shortened, and the electric loading is increased to compensate, this will cause higher iron and magnet losses.

The simulations that produced Fig. 15 were repeated for the ferrite and sintered NdFeB options with the stack length increased to 150 mm (see Fig. 16). Interestingly the bonded NdFeB option has the highest minimum loss, while the ferrite and sintered NdFeB options have roughly the same minimum loss. The reason for this is not clear and requires further investigation. The "optimal" stack length corresponding to minimum loss appears to vary roughly inversely with remanent flux density.

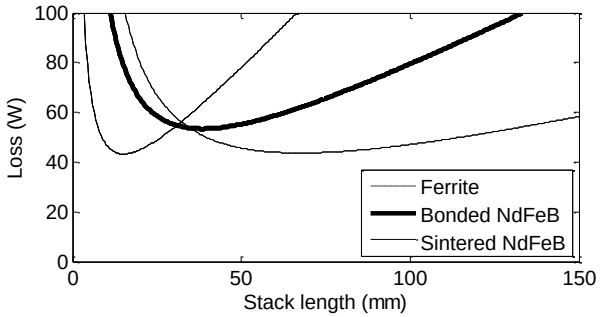

Fig. 16. Loss against stack length for the three options at 400 W and 3000 rpm

The material costs are linearly proportional to stack length (ignoring the effects of end-windings), so plots of loss against load for varying stack lengths can be used to obtain a plot of loss against cost. Fig. 17 shows the plot for the three options at rated power. Their shape is similar to that of the plot of loss against stack length, with the horizontal axis values scaled by the relative costs.

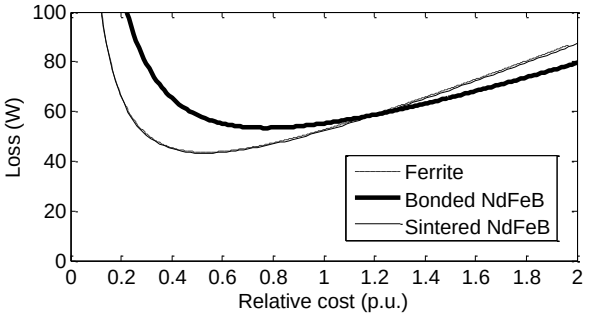

Fig. 17. Loss against cost for the three options at 400 W and 3000 rpm. The cost is normalized against the bonded NdFeB magnet machine with a 50 mm stack length.

It was found that the sintered NdFeB option curve has a nearly identical shape to that of the ferrite option. The base line bonded NdFeB design has the highest minimum loss at a higher cost, but then the loss increases more gradually with cost than the other two options.

For low values of loss (say 60 W), the bonded option cost is nearly 2.5 times higher than that of the ferrite and sintered option. At mid-range loss (say 80 W), the bonded option cost is nearly 2 times that of the ferrite and sintered options.

For low values of cost (say 0.4 p.u.), the ferrite and sintered options have much lower loss than the bonded option. For a mid-range cost (say 1.3 p.u.), all three options have about the same loss, while at higher costs (say 2 p.u.), the bonded option has the lowest loss, followed by the sintered and ferrite options.

The above simplified analysis has neglected the effect of the 3D SMC machine geometry which complicates both the analysis and the implementation of stack length changes. This will be investigated in future work.

V. Conclusions

This paper presented the modelling and experimental testing of a brushless SMC based PM machine. Three options for the rotor magnet were considered: a bonded NdFeB ring, a sintered NdFeB magnet, and a ferrite magnet. A prototype SMC machine with a bonded NdFeB magnet ring was constructed and FE modelled. The model was verified experimentally and used to compare the three rotor magnet options.

A simplified analytical study was performed on the effect of changing the magnet remanent flux and the stack length on the total losses of the machine. In particular, the loss versus material cost curves were calculated at rated power and speed for each of the magnet options when the stack length was varied.

It was found that at rated power, the optimized stack length ferrite and sintered NdFeB options have the lowest minimum loss and have comparable values of material cost. The bonded NdFeB option has a higher minimum loss and this occurs at a higher value of cost.

Further work is required to investigate the reason for the differences in the value of minimum loss for three rotor designs and to take into account the 3D nature of the SMC teeth in the optimization.

VI. Acknowledgment

The authors gratefully acknowledge the support of the Australian Research Council (ARC Project LP120200755) and the industrial partner Intelligent Electric Motor

Solutions (IEMS) Pty. Ltd. The authors would also like to thank the staff of the School of Electrical and Electronic Engineering Workshop for their help with constructing the machine and the experimental setup.

VII. REFERENCES

[1] L. O. Hultman and A. G. Jack, "Soft magnetic composites-materials and applications," *IEEE International Electric Machines and Drives Conference*, Madison, Wisconsin, USA, 2003.

[2] C. Tang, W.L. Soong, G.S. Liew and N. Ertugrul, "Modelling of surface PM machine using soft magnetic composites and a bonded magnet ring," *2012 XXth International Conference on Electrical Machines*, Marseille, France, 2012.

[3] S. Eriksson and H. Bernhoff, "Rotor design for PM generators reflecting the unstable neodymium price," *2012 XXth International Conference on Electrical Machines*, Marseille, France, 2012.

[4] Y. Takano, M. Takeno, T. Imakawa, A. Chiba, N. Hoshi, M. Takemoto, S. Ogasawara, "Torque density and efficiency improvements of a Switched Reluctance Motor without rare earth material for hybrid vehicles," 2010 IEEE Energy Conversion Congress and Exposition, Atlanta, Georgia, USA, 2010.

[5] I. Petrov and J. Pyrhonen, "Performance of Low-Cost Permanent Magnet Material in PM Synchronous Machines," *IEEE Transactions on Industrial Electronics*, vol. 60, no. 6, pp. 2131-2138, 2013.

[6] M. Barcaro, N. Bianchi and F. Magnussen, "Permanent-magnet optimisation in permanent-magnet-assisted synchronous reluctance motor for a wide constant-power speed range," *IEEE Transactions on Industrial Electronics*, vol. 59, no. 6, pp. 2495-2502, 2012.

[7] M. Barcaro and N. Bianchi, "Interior PM machines using ferrite to replace rare-earth surface PM machines," *IEEE Transactions on Industry Applications*, vol. 50, no. 2, pp. 979-985, 2014.

[8] D. Zarko and S. Stipetic, "Criteria for optimal design of interior permanent magnet motor series," *2012 XXth International Conference on Electrical Machines*, Marseille, France, 2012.

VIII. BIOGRAPHIES

Yik Ling Lim (S'08) received the B.Sc. degree in mathematics and computer science, B.Eng. degree (with honours) in computer systems engineering and M.Phil. degree in electrical and electronic engineering from the University of Adelaide, Australia, in 2002, 2007 and 2013, respectively. She commenced the Ph.D. degree study at the University of Adelaide in September 2013. Her research interests include the design of permanent magnet machines using soft magnetic composite materials and sensorless control strategies for wind turbine generator systems.

Wen L. Soong (S'89–M'93) was born in Kuala Lumpur, Malaysia. He received the B.Eng. degree from the University of Adelaide, Australia, in 1989, and the Ph.D. degree from the University of Glasgow, U.K., in 1993.

He worked at General Electric Corporate Research and Development, Schenectady, New York, before joining the University of Adelaide, in 1998. His research interests include permanent magnet and reluctance machines, renewable energy generation, and condition monitoring.

Nesimi Ertugrul (M'95) received the B.Sc. degree in electrical engineering and the M.Sc. degree in electronic and communication engineering from the Istanbul Technical University, Turkey, in 1985 and 1989 respectively, and the Ph.D. degree from the University of Newcastle, Newcastle upon Tyne, U.K., in 1993.

He has been with the University of Adelaide since 1994, where he is an Associate Professor. His primary research topics include sensorless operation of switched machines, power electronics, renewable energy systems, fault-tolerant motor drives, power quality monitoring and condition monitoring. He is the author of a book, *LabVIEW for Electric Circuits, Machines, Drives, and Laboratories* (Prentice-Hall, 2002).

Gabriel Haines received the B.E. degree (with honours) in electrical and electronic engineering from the University of Adelaide, Adelaide, Australia, in 2012. He is currently a part time research engineer with the power electronics and control group at the University of Adelaide. His research interests include power electronics, integrated motor control systems and energy storage systems.